Available online at www.sciencedirect.com
SCIENCE DIRECT®
Journal of Power Sources 146 (2005) 15–20
JOURNAL OF POWER SOURCES
www.elsevier.com/locate/jpowsour

Advanced in situ characterization methods applied to carbonaceous materials

P. Novák *, D. Goers, L. Hardwick, M. Holzapfel, W. Scheifele, J. Ufheil, A. Würsig

Paul Scherrer Institut, Electrochemistry Laboratory (Member of the ALiSTORE Network of Excellence), CH-5232 Villigen PSI, Switzerland

Available online 31 May 2005

Abstract

This paper is an overview of the progress recently achieved in our laboratory in the development and application of four in situ methods; namely X-ray diffraction (both synchrotron-based and standard), Raman microscopy, differential electrochemical mass spectrometry (DEMS), and infrared spectroscopy. We show representative results on graphite electrodes for each method as an illustration, in particular (i) the influence of the lithium intercalation and graphite exfoliation on the shift of the (0 0 2)-reflection of graphite, (ii) Raman single point and mapping measurements of graphite surface, (iii) gas evolution during solid electrolyte interphase (SEI) formation on graphite electrodes, and (iv) the development of infrared spectra during the SEI formation in γ-butyrolactone based electrolytes.

Keywords: Lithium-ion battery; Graphite electrode; In situ X-ray diffraction; In situ Raman mapping; In situ mass spectrometry; In situ infrared spectroscopy

1. Introduction

In lithium-ion batteries, carbonaceous materials are used in both electrodes. In the negative electrode the carbonaceous material stores lithium ions [1]. Nowadays, artificial graphite is used in advanced batteries [2]. It is the preferred material on account of low cost, low irreversible charge capacity, outstanding cycling stability, and ability to provide very high currents [3]. (Micro)structural parameters [4] have a strong influence on the lithium intercalation mechanism into carbons and affect their electrochemical behavior [5]. Moreover, the electrode potential of lithiated carbon is far beyond the thermodynamic stability window of the most commonly used organic electrolytes. Hence, the electrolyte (either liquid or gelled) is reduced forming at the surface of the negative electrode material a layer called the solid electrolyte interphase (SEI) [6]. In most cases gas is formed at the carbon/electrolyte interface at the same time [7–9]. Fortunately, the SEI, once formed, normally prevents further reductive electrolyte decomposition and gas formation. A clear identification of the SEI composition and its formation mechanism(s) is important for thorough understanding and optimization of lithium-ion batteries. The SEI layer consists of decomposition products of electrolyte salt and solvent(s) [1,6,10–17]. Models assume that the SEI is composed of two major constituents described as inorganic and organic interpenetrating layers [1]. The composition of the inorganic layer is fairly well understood. But complete understanding of the organic layer remains a challenge because of the inevitable exposure of the SEI film to air and/or vacuum which occurs when using common analytical methods. This results in a loss of volatile (organic) components, shrinkage of the film, and even in changes in the chemistry of the film. Hence, the use of in situ analytical tools is advantageous. In the following text, an overview will be presented of the progress achieved in our laboratory in the development and application of suitable in situ methods during the last five years since our first overview was published [18]. For each method, the corresponding electrochemical cell will be depicted and a representative result will be reported.

2. In situ X-ray diffraction

Due to the reversible lithium intercalation into graphite the interlayer distance between the graphene layers increases moderately (10.3% was calculated for LiC_6) [1,4,19]. In

* Corresponding author. Tel.: +41 56 310 2457; fax: +41 56 310 4415.
E-mail address: petr.novak@psi.ch (P. Novák).

0378-7753/$ – see front matter © 2005 Elsevier B.V. All rights reserved.
doi:10.1016/j.jpowsour.2005.03.129

contrast, in the case of irreversible processes one can observe either strong lattice expansion (due to solvated intercalation [20]) or no lattice change (due to cracking of the particles and electrical isolation of most of the active mass by SEI films due to strong electrolyte decomposition [21]). In situ X-ray diffraction (XRD) is a powerful tool to monitor the structural evolution of active battery materials during cycling without the risk of contamination or degradation of the materials. In the particular case of lithium intercalation into graphite the XRD method provides information on the reversibility of the intercalation process. However, great care must be exercised in designing the cell. This is because XRD probes the bulk of the particles while their potential is determined by the lithium concentration at the particle surface. Thus, rapid equilibration of the entire insertion electrode should be achieved in a well-designed cell. Consequently, the current density distribution over the surface of the working electrode should be uniform, while the internal resistance of the cell should be minimized.

The use of synchrotron light is particularly suited because the X-ray beam shows a very high intensity and its wavelength can be tuned. The PSI synchrotron is unique in this context because of its very high beam stability, admitting for long time measurement series without difficulties in data analysis. The high intensity of the beam allows the use of a standard electrochemical arrangement without compromising the electrochemical properties of the cell. In our case we use "coffee-bag" type cells (Fig. 1) with copper grids as current collectors for both, the graphite working electrode and the lithium counter electrode. (For experiments on positive electrode materials an aluminum grid current collector is used.) The collection is very fast; one diffraction pattern can be normally recorded within 5–20 s. As an example we present in Fig. 2 a synchrotron in situ X-ray diffraction study on a standard graphite electrode in a standard battery electrolyte, 1 M $LiPF_6$ in EC/DMC (1:1, w/w). Indeed, the (0 0 2)-reflection of graphite shifts to lower reflection angles during lithium intercalation. The observed line shift confirms the intercalation of naked lithium ions without their solvation shells into the graphite indicating a highly reversible intercalation process.

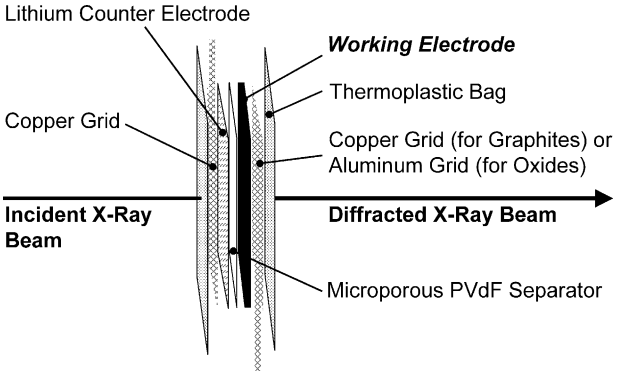

Fig. 1. The electrochemical cell for in situ X-ray diffraction using synchrotron light.

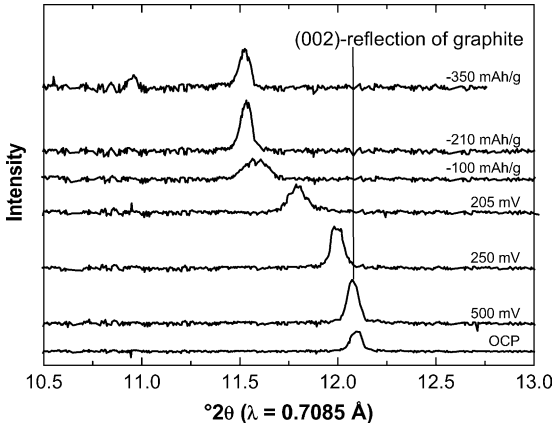

Fig. 2. In situ synchrotron X-ray diffraction patterns of standard graphite; electrolyte 1 M $LiPF_6$ in EC/DMC (1:1, w/w); all quoted potentials are vs. Li/Li^+; OCP = open circuit potential.

Apart from the very fast spectra collection, the synchrotron-based technique faces two major challenges, the availability of the beam and the very high cost of the synchrotron beam time. A number of X-ray diffraction studies can be performed with a standard laboratory diffractometer as well. However, the cell must be modified and the time necessary for recording one diffraction pattern is significantly longer. Our in situ cell (Fig. 3) has an internal arrangement which resembles that of a coin cell. Thus, the current density on the working electrode is uniform. The material of the cell body is PEEK (poly ether ether ketone) polymer which is stable in all relevant electrolytes. The beam attenuation due to the PEEK material is minor in comparison to the X-ray absorption in the electrolyte solution. Moreover, there are no diffraction patterns from the PEEK but a broad band at ca.

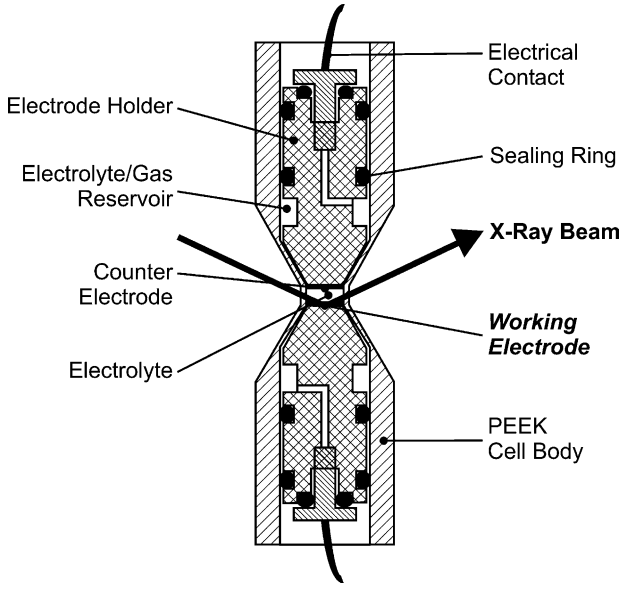

Fig. 3. The electrochemical cell for in situ X-ray diffraction using a standard laboratory diffractometer.

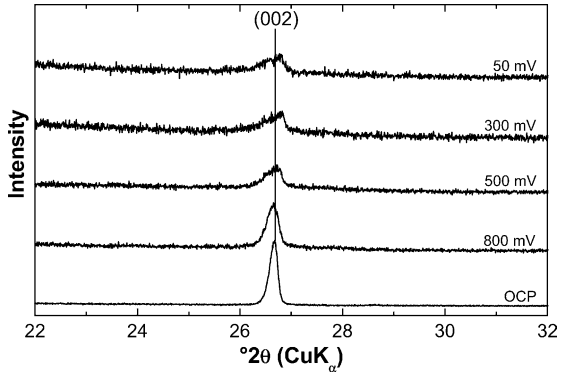

Fig. 4. In situ X-ray diffraction patterns of entirely hexagonal graphite; electrolyte 1 M $LiPF_6$ in EC/PC (1:1, w/w); all quoted potentials are vs. Li/Li^+; OCP = open circuit potential.

10° only, thus, all relevant bands from the graphite (or other materials) can be analyzed.

Fig. 4 shows as an example the development of the X-ray diffraction patterns with decreasing potential of a special graphite with entirely hexagonal structure (for sample preparation see [5]) in a propylene carbonate (PC) based electrolyte. One diffraction pattern was recorded within ca. 42 min in this case. No shift of the (0 0 2) Bragg reflection of graphite can be observed. Peak broadening and decrease of the peak magnitude, indicating amorphization, can be ascribed to irreversible graphite exfoliation showing that this process takes place instead of lithium intercalation.

3. In situ Raman microscopy

The surface of graphite electrodes is extremely disorganized on the micrometer scale. In order to produce the optimum graphite electrode a better evaluation of these variations needs to be undertaken. The L_a value is an important parameter of graphite which provides a measure of local surface disorder and represents the length of the graphene crystallite sheets. It is derived from the ratio of the areas of the G and D Raman band (the E_{2g} and A_{1g} mode, respectively) and then calculated using the Tuinstra and Koenig equation [22]. (For experimental details see [23].) The volume resolution of confocal Raman microscopy achieved in our laboratory is approaching 1 μm^3, thus, the Raman analysis (ex situ and in situ) of the electrode's surface heterogeneity is possible. Defects on the surface of single carbon particles can be visualized by point mapping of graphite electrodes with a high number of data points. Results show that it is possible to "image" electrodes using their L_a values and, therefore, show the correlation of L_a with the morphology of the surface of the electrode (Fig. 5).

In Fig. 6, we show the schematic drawing of the in situ Raman cell developed by us, where all kinds of electroactive materials can be used as test samples. The cell is an improved model of a previous design described elsewhere [24]. The use of electrodes which possess a small hole in the current collector permits backside viewing of the working electrode and so allows measurements next to the optical window. This results in better resolution and eliminates problems of measuring through the electrolyte. A drop of the electroactive material (in a slurry) is placed onto a pre-hole-punched current collector (hole diameter <1 mm), dried, and weighed (<1 mg active mass). The cell consists of a lithium or oxide counter electrode, a separator, and a "holed" graphite working electrode. The working electrode is observed from the rear through a thin (0.1 mm) glass optical window. An arbitrary area of the electrode is chosen and brought into focus. The image of the electrode is recorded, and the CCTV and XYZ table working

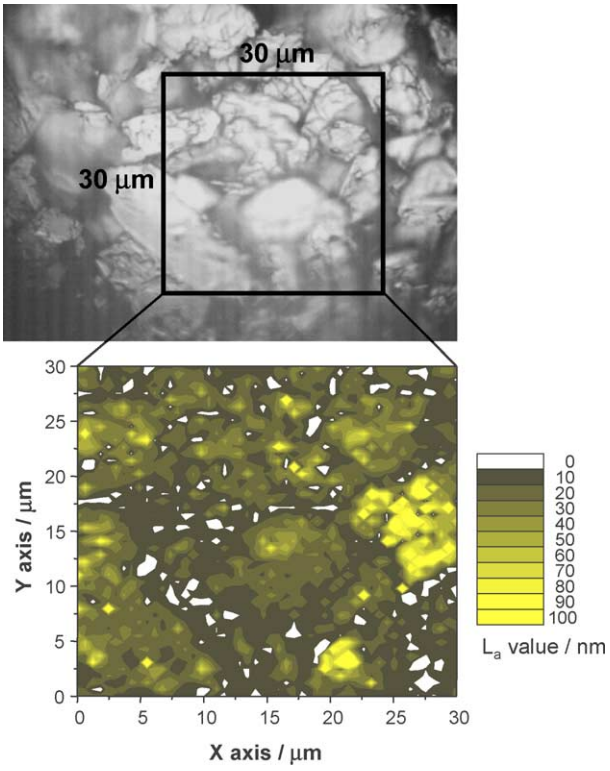

Fig. 5. Raman mapping of graphite surface: Image of a graphite sample (top) and spatial distribution plot of the L_a values (bottom, map 50 × 50 points). Bad data points are shown in white (ca. 5% of spectra); resolution approaching 1 μm^3.

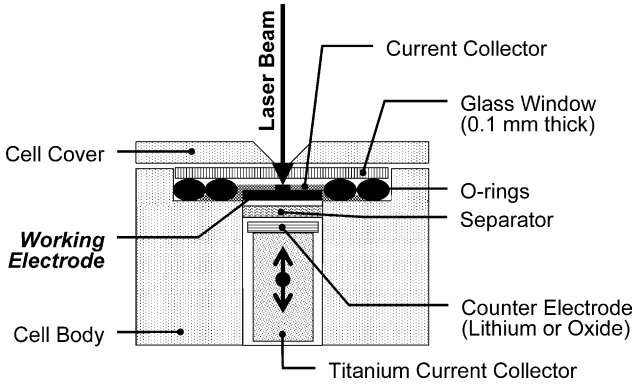

Fig. 6. The electrochemical cell for in situ Raman microscopy.

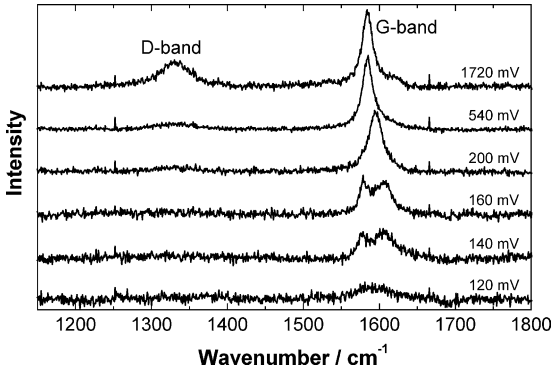

Fig. 7. In situ Raman spectra of the first lithium intercalation into graphite. Single point measurement under confocal conditions; 2–3 μm^3 resolution using 80× objective with HeNe Laser 632.8 nm with ca. 1 mW laser power; 300 s; 1 accumulation per spectrum; electrolyte 1 M $LiClO_4$ in EC/DMC (1:1, w/w); all quoted potentials are vs. Li/Li^+.

with an autofocus unit allows strict position control throughout the measurements. The spectra in Fig. 7 confirm that the signal-to-noise ratio of useful bands in single point (2–3 μm^3 resolution) in situ Raman spectra is very good even if only one accumulation per spectrum is used for spectra collection. The Raman signals from the electrolyte are negligible.

The traces shown in Fig. 7 illustrate the changes observed in the in situ Raman spectra upon lithium intercalation into graphite. The spectra were recorded at the same location of the electrode surface during the first charging half-cycle. For the lithium-free carbon both, the D and G bands are clearly visible. During lithium intercalation (i.e., with decreasing potential) the G band shifts to higher wavenumbers and splits in two components in agreement with the observations previously reported [24–26]. A disappearance of the D band with decreasing potential of the carbon was observed as well.

4. Differential electrochemical mass spectrometry

With the differential electrochemical mass spectrometry (DEMS) technique it is possible to detect the various gaseous reaction products that are evolved during the SEI film formation and/or the electrode cycling [8]. Hence, intensity changes in mass signals (mass-spectrum cyclic voltammograms, MSCV) can be detected as a function of time and/or potential and, thus, can be correlated with current peaks in the cyclic voltammograms (CV) or plateaus on galvanostatic charging/discharging curves. The amounts of major gaseous reaction products (typically hydrogen, ethylene, and/or propylene) are rather high. However, for answering the question if additional gases such as CO_2 are developed during the cycling of lithium-ion batteries, the previously used DEMS measurement cell [18,27] had to be considerably improved. The new measurement system shown in Fig. 8 is based on headspace analysis. The gaseous reaction products are pumped off continuously from the top of the electrochemical cell via a capillary into a quadrupole mass spectrometer

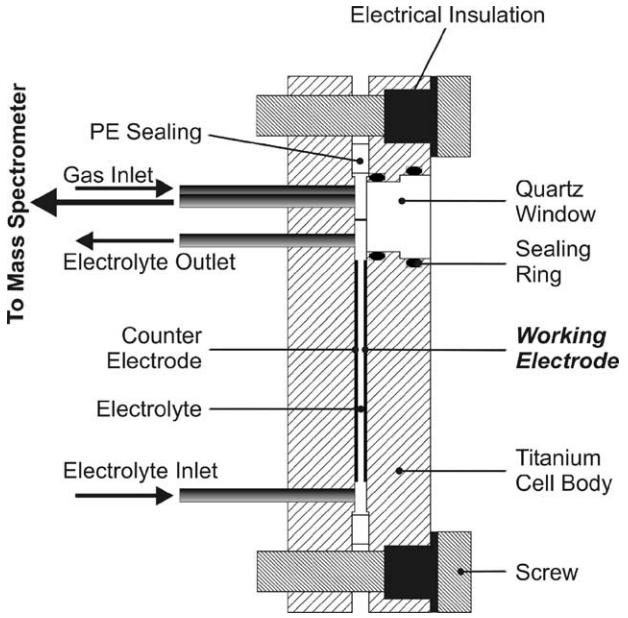

Fig. 8. The electrochemical cell for in situ DEMS.

where they are analyzed on line. With this electrochemical cell it is now possible to identify much smaller quantities of gas. Furthermore, a full quantitative gas analysis is feasible. The cell can also be adapted for measurements at elevated temperature and for half-cell as well as full-cell investigations.

As an example, DEMS results showing gas evolution on graphite electrodes during the SEI formation in the presence of a new additive, maleic anhydride (MA) in γ-butyrolactone (GBL) based electrolytes are shown in Fig. 9. (The details on the MA additive are published in [28].) Hydrogen and carbon dioxide were detected during the first electrochemical cycles. Hydrogen is observed in both, MA free and MA containing electrolytes. Thus, the evolution of H_2 is assigned to the reductive decomposition of GBL. On the contrary, the CO_2 gas was detected in MA containing electrolytes only. The reason for the large amount of the CO_2 evolved in the first cycle is most likely the reductive decomposition of MA at higher potentials and, in addition, the decomposition of GBL in the presence of MA at lower potentials. In the second cycle the H_2 evolution is stronger but the development of CO_2 does not start before 0.35 V versus Li/Li^+ (Fig. 9). Apparently, the graphite surface is more active in the second cycle, possibly due to an amorphization process, resulting in a more positive decomposition potential for GBL. As in the second cycle no more CO_2 is evolved at higher potentials, the MA degradation seems to be completed. The remaining CO_2 production originates from the GBL degradation [28].

5. In situ infrared spectroscopy

A method highly complementary to DEMS is in situ infrared spectroscopy. Due to its molecular specificity it is

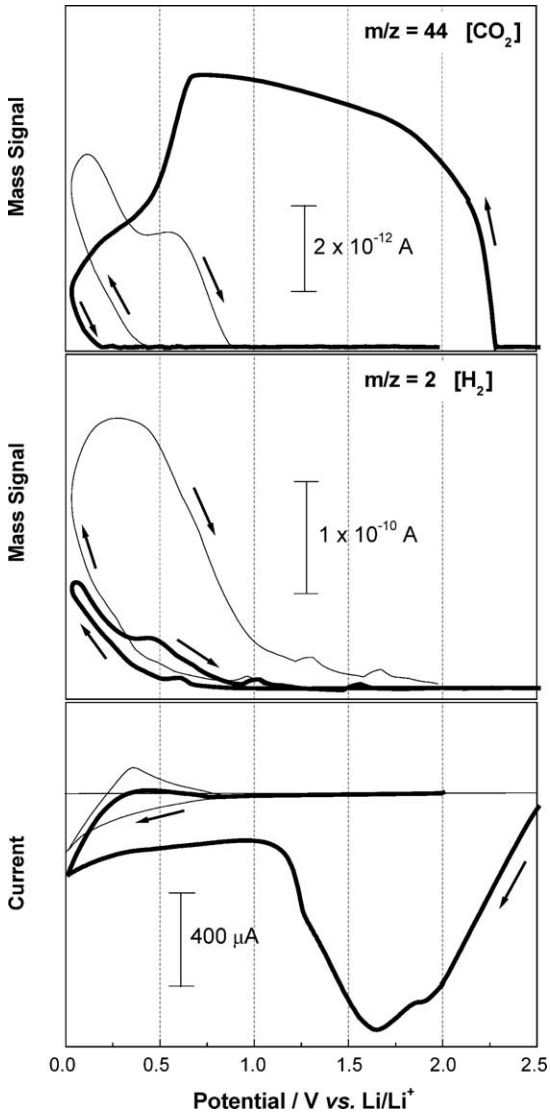

Fig. 9. In situ DEMS experiment showing first two cycles of a graphite electrode in the electrolyte 1 M $LiBF_4$ in GBL + 2% MA (bottom, CV; top and center, two MSCVs; bold lines, first cycle; thin lines, second cycle). The MSCVs exhibit mass signals $m/z = 44$ and $m/z = 2$, representing carbon dioxide and hydrogen, respectively. The scan rate was 0.4 mV s^{-1}.

highly suitable for the analysis of interface processes like SEI formation. Two major challenges are faced. Firstly, the electrolyte solution strongly absorbs infrared light. Thus, thin-layer external reflectance or, alternatively, internal reflectance techniques must be used [18]. Secondly, there is a problem of sensitivity if very low absorptions from species on or near an electrode have to be detected. This problem can be overcome by subtracting spectra recorded at different potentials. Under optimum conditions the sensitivity of infrared detection of, e.g., CO_2 is much higher then with the DEMS [29].

Our experimental approach is based on the SNIFTIRS (Subtractively Normalized Interfacial Fourier Transform Infrared Spectroscopy) technique. A hermetically sealed spectro-electrochemical cell designed for measurements in water and oxygen-free environment is used (Fig. 10). It is a

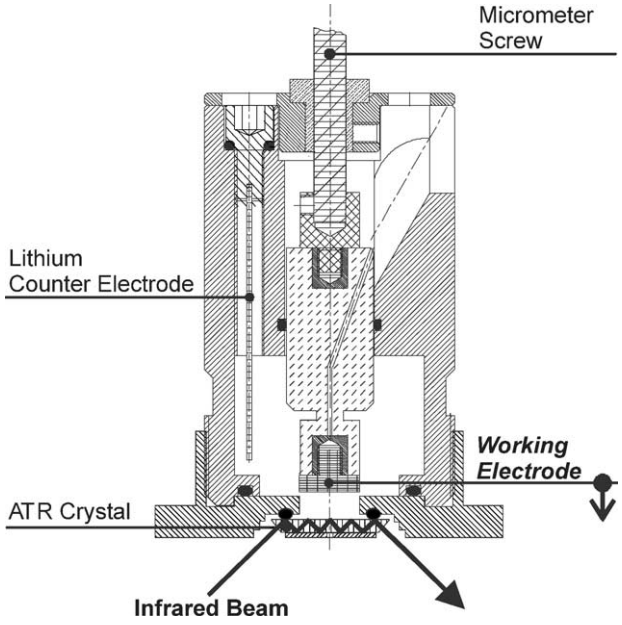

Fig. 10. The electrochemical cell for in situ infrared spectroscopy with the working electrode shown in the position back from the optical window.

thin layer, one-compartment cell with the working electrode pushed against the optical window. The cell is installed in the FTIR spectrometer with the surface of the working electrode in a horizontal position. Thus, the amount of the electrolyte is minimized. The construction details of the cell are the same as published by us elsewhere [18,30] but the decisive innovation is the use of an ATR crystal (made from ZnSe in our case) as the optical window. In our arrangement five reflections can be used increasing, thus, the sensitivity significantly. The working electrode is a mechanically polished glassy carbon (GC) disc, optionally spray-coated with a thick layer of, e.g., graphite with binder. Alternatively, the working electrode is made from any suitable polished metal. The potential-dependent changes at the electrode/electrolyte interface and in the thin electrolyte layer between the electrode and the optical window are visualized by plotting R_E/R_0, where R_E is the single beam spectrum recorded

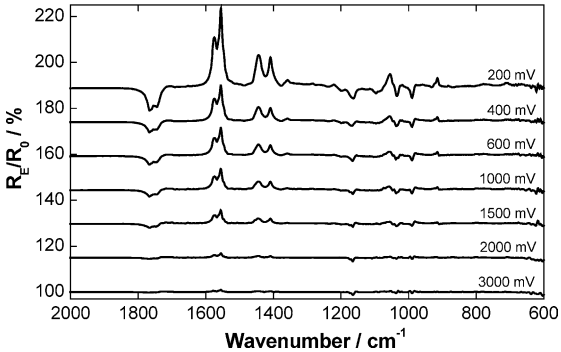

Fig. 11. In situ infrared spectra (SNIFTIRS-ATR) from a polished GC electrode ($d = 13$ mm) in the electrolyte 1 M $LiClO_4$ in GBL. The scan rate was 0.2 mV s^{-1}; all quoted potentials are vs. Li/Li^+. The spectra were arbitrarily shifted on the vertical scale.

at the working electrode potential and R_0 the background single beam spectrum recorded usually at the open-circuit potential. In Fig. 11 a typical result is shown – the potential dependence of the SNIFTIR spectra for the reduction of GBL with 1 M $LiClO_4$. Positive-going and negative-going bands represent a decrease or increase, respectively, in the concentration of species at the electrode or in the thin electrolyte layer between the electrode and the optical window. The assignment of the bands is discussed in Ref. [28].

Acknowledgments

The financial support of the Swiss National Science Foundation, the Swiss Federal Office of Education and Science (European Project CAMELiA), and the TIMCAL SA is gratefully acknowledged. M. Spahr (TIMCAL SA, Bodio, Switzerland), H. Buqa (PSI), J. Vetter (PSI), A. Wokaun (PSI), and B. Schmitt (PSI–SLS) are acknowledged for fruitful discussions and/or contributions to the method development. M. Morcrette (LRCS, Amiens, France) is acknowledged for his valuable contribution to the assembly of the “coffee-bag” type cells used in synchrotron X-ray experiments.

References

[1] M. Winter, J.O. Besenhard, M.E. Spahr, P. Novák, Adv. Mater. 10 (1998) 725–763.
[2] M. Broussely, P. Blanchard, P. Biensan, J.P. Planchat, K. Nechev, R.J. Staniewicz, J. Power Sources 119–121 (2003) 859–864.
[3] H. Buqa, D. Goers, M.E. Spahr, P. Novák, ITE Batt. Lett. 4 (2003) 38–43.
[4] D. Billaud, F.X. Henry, Solid State Commun. 124 (2002) 299–304.
[5] M.E. Spahr, H. Wilhelm, F. Joho, J.C. Panitz, J. Wambach, P. Novák, N. Dupont-Pavlovsky, J. Electrochem. Soc. 149 (2002) A960–A966.
[6] E. Peled, D. Golodnitsky, C. Menachem, D. BarTow, J. Electrochem. Soc. 145 (1998) 3482–3486.
[7] R. Imhof, P. Novák, Proceedings of the First Joint Meeting of the Electrochemical Society/International Society of Electrochemistry, Paris, France, August 31–September 05, 1997, Electrochemical Society Inc., 1997, pp. 313–323.
[8] R. Imhof, P. Novák, J. Electrochem. Soc. 145 (1998) 1081–1087.
[9] J.S. Shin, C.H. Han, U.H. Jung, S.I. Lee, H.J. Kim, K. Kim, J. Power Sources 109 (2002) 47–52.
[10] D. Aurbach, B. Markovsky, A. Shechter, Y. Ein Eli, H. Cohen, J. Electrochem. Soc. 143 (1996) 3809–3820.
[11] D. Aurbach, B. Markovsky, M.D. Levi, E. Levi, A. Schechter, M. Moshkovich, Y. Cohen, J. Power Sources 82 (1999) 95–111.
[12] E. Peled, D.B. Towa, A. Merson, L. Burstein, J. New Mater. Electrochem. Syst. 3 (2000) 319–326.
[13] D. Aurbach, J. Power Sources 89 (2000) 206–218.
[14] P. Novák, F. Joho, M. Lanz, B. Rykart, J.C. Panitz, D. Alliata, R. Kötz, O. Haas, J. Power Sources 97/98 (2001) 39–46.
[15] H. Ota, T. Sato, H. Suzuki, T. Usami, J. Power Sources 97/98 (2001) 107–113.
[16] Y.X. Wang, P.B. Balbuena, J. Phys. Chem. A 106 (2002) 9582–9594.
[17] D. Aurbach, J. Power Sources 119 (2003) 497–503.
[18] P. Novák, J.C. Panitz, F. Joho, M. Lanz, R. Imhof, M. Coluccia, J. Power Sources 90 (2000) 52–58.
[19] D. Billaud, F.X. Henry, M. Lelaurain, P. Willmann, J. Phys. Chem. Solids 57 (1996) 775–781.
[20] M. Winter, G.H. Wrodnigg, J.O. Besenhard, W. Biberacher, P. Novák, J. Electrochem. Soc. 147 (2000) 2427–2431.
[21] D. Aurbach, M. Koltypin, H. Teller, Langmuir 18 (2002) 9000–9009.
[22] F. Tuinstra, J.L. Koenig, J. Chem. Phys. 53 (1970) 1126–1130.
[23] D. Goers, H. Buqa, L. Hardwick, A. Würsig, P. Novák, Ionics 9 (2003) 258–265.
[24] J.C. Panitz, P. Novák, O. Haas, Appl. Spectrosc. 55 (2001) 1131–1137.
[25] M. Inaba, H. Yoshida, Z. Ogumi, T. Abe, Y. Mizutani, M. Asano, J. Electrochem. Soc. 142 (1995) 20–26.
[26] J.C. Panitz, F. Joho, P. Novák, Appl. Spectrosc. 53 (1999) 1188–1199.
[27] R. Imhof, P. Novák, J. Electrochem. Soc. 146 (1999) 1702–1706.
[28] J. Ufheil, M.C. Bärtsch, A. Würsig, P. Novák, Electrochim. Acta 50 (2005) 1733–1738.
[29] M. Winter, R. Imhof, F. Joho, P. Novák, J. Power Sources 82 (1999) 818–823.
[30] F. Joho, P. Novák, Electrochim. Acta 45 (2000) 3589–3599.